

Dinuclear organometallic dinitrogen complexes of niobium

Michael D. Fryzuk*, Christopher M. Kozak, Brian O. Patrick¹

Department of Chemistry, University of British Columbia, 2036 Main Mall, Vancouver, British Columbia, Canada V6T 1Z1

Received 29 April 2002

Dedicated to Professor Richard R. Schrock in honour of his contributions to inorganic chemistry, particularly in the field of dinitrogen activation

Abstract

The niobium(III) chloride precursors $^R[P_2N_2]NbCl$ stabilized by the bis-(amidophosphine) macrocycle (where $^R[P_2N_2] = RP(CH_2SiMe_2NSiMe_2CH_2)_2PR$, R = phenyl, Ph, or cyclohexyl, Cy), react with MeMgCl under argon to form the paramagnetic $^R[P_2N_2]NbMe$ (R = Ph, **1**; R = Cy, **2**) complexes. The methyl complexes **1** and **2** can be stabilized by the donor solvent pyridine to form the paramagnetic adducts $^R[P_2N_2]NbMe(py)$ (R = Ph, **3**; R = Cy, **4**). Methyl complexes **1** and **2** readily react with N_2 to form the diamagnetic dinuclear dinitrogen compounds, $(^R[P_2N_2]NbMe)_2(\mu-N_2)$ (R = Ph, **5**; R = Cy, **6**), which have been characterized crystallographically. Dinitrogen complex **5** is fluxional and undergoes enantiomeric inversion of the six-coordinate niobium centres via axial rotation about the Nb–N₂–Nb axis. Complex **6** shows no enantiomeric inversion, likely due to the steric effects of the cyclohexyl substituents. The dinitrogen ligand itself is labile at elevated temperatures and undergoes reversible dissociation; the dinitrogen complexes are reformed upon cooling to room temperature. Reaction of **5** and **6** with CO displaces the N₂ fragment forming the bridging acyl complexes $(^R[P_2N_2]Nb)_2(\mu-COCH_3)_2$ (R = Ph, **7**; R = Cy, **8**) where the carbonyl fragments bond to the metal centres in a η^2 fashion. Addition of H₂ to **5** and **6** results in the formation of the previously reported paramagnetic dinuclear dinitrogen complex, $(^R[P_2N_2]Nb)_2(\mu-N_2)$.

© 2002 Elsevier Science B.V. All rights reserved.

Keywords: Dinitrogen complexes; Niobium; Crystallography; Amidophosphine ligands; Macrocycles; Fluxionality

1. Introduction

The activation of molecular nitrogen by transition metal complexes has been an active area of research for almost four decades [1–3]. However, the synthesis of complexes that contain coordinated dinitrogen is still considered difficult and oftentimes fortuitous. The most common method to synthesize a dinitrogen compound involves reduction of a precursor derivative in the presence of N₂. However, this technique does not guarantee dinitrogen complex formation and often complicated side reactions ensue [4].

We have recently reported the synthesis of a paramagnetic diniobium dinitrogen compound by reduction

of a Nb(III) chloride precursor. Reaction of $^R[P_2N_2]NbCl$ (where $^R[P_2N_2] = RP(CH_2SiMe_2NSiMe_2CH_2)_2PR$, R = Ph) with potassium graphite (KC₈) under dinitrogen generates the bridging dinitrogen complex $(^{Ph}[P_2N_2]Nb)_2(\mu-N_2)$ [5]. We have also reported the synthesis of stable monomeric high-spin niobium(III) alkyl complexes of the formula $^R[P_2N_2]NbR'$ (where R = Ph or Cy, and R' = CH₂SiMe₃ or CH(SiMe₃)₂) [6]. If the stability of these alkyl species is due to the bulky nature of the alkyl groups, then it was of interest to explore the reactivity of the much less sterically demanding niobium–methyl complexes. The high Lewis acidity demonstrated by niobium(III) species in concert with the more accessible metal centre allowed by the small methyl ligand would likely generate much more reactive species as compared to the bulkier analogs. In this work we present the syntheses of the paramagnetic niobium–methyl complexes $^R[P_2N_2]NbMe$ and their ability to readily bind dinitrogen.

* Corresponding author. Tel.: +1-604-822 2897; fax: +1-604-822 2847.

E-mail address: fryzuk@chem.ubc.ca (M.D. Fryzuk).

¹ UBC X-ray Structural Chemistry Laboratory.

2. Experimental

2.1. General

Unless otherwise stated, all manipulations were performed under an atmosphere of dry oxygen-free nitrogen or argon by means of standard Schlenk or glovebox techniques (Vacuum Atmospheres HE-553-2 glovebox equipped with a MO-40-2H purification system and a $-40\text{ }^{\circ}\text{C}$ freezer). Hexanes and toluene were purchased anhydrous from Aldrich and further dried by passage through a tower of alumina and degassed by passage through a tower of Q-5 catalyst under positive pressure of nitrogen [7]. Anhydrous diethyl ether and THF were stored over sieves and distilled from sodium benzophenone ketyl under argon. Pyridine was dried by refluxing over CaH_2 under nitrogen. Nitrogen and argon were dried and deoxygenated by passage through a column containing molecular sieves and MnO. Deuterated benzene and toluene were dried by refluxing over sodium and potassium alloy in sealed vessels under partial pressure followed by trap-to-trap distillation. They were degassed under three freeze–pump–thaw cycles. Unless otherwise stated, all NMR spectra were recorded on a Bruker AMX-500 instrument operating at 500.132 MHz for ^1H spectra. ^1H NMR spectra were referenced to residual protons in the deuterated solvent. FTIR spectra were recorded on a BOMEM MB 100 spectrophotometer. Elemental analyses were performed by Mr. P. Borda of this department. Mass Spectrometry was performed on a Kratos MS 50 by Mr. M. Lapawa, also of this department. MeMgCl was purchased from Aldrich as a 3.0 M solution in THF and used as received. CO gas was purchased from Matheson and H_2 purchased from Praxair. Both were used without further purification.

2.2. Synthesis

2.2.1. $^{\text{Ph}}[\text{P}_2\text{N}_2]\text{NbMe}$ (1)

MeMgCl (0.25 ml, 0.760 mmol) was slowly added to a stirred solution of $^{\text{Ph}}[\text{P}_2\text{N}_2]\text{NbCl}$ (500 mg, 0.760 mmol) in toluene (25 ml) under argon to produce an immediate colour change from green to dark purple. After stirring for 6 h, solvents were removed in vacuo to produce a purple residue. The residue was extracted with toluene and filtered through Celite. Removal of toluene afforded a paramagnetic purple solid that was washed with hexanes to give an analytically pure product. Yield 430 mg (88%). *Anal.* Calc. for $\text{C}_{25}\text{H}_{45}\text{N}_2\text{NbP}_2\text{Si}_4$: C, 46.86; H, 7.08; N, 4.37. Found: C, 46.49; H, 7.17; N, 4.69%. MS (EI) m/z (%) 640, (80) $[M]^+$. μ_{eff} (Evans method) = $2.5\ \mu_{\text{B}}$.

2.2.2. $^{\text{Cy}}[\text{P}_2\text{N}_2]\text{NbMe}$ (2)

$^{\text{Cy}}[\text{P}_2\text{N}_2]\text{NbMe}$ was synthesized according to the procedure used for $^{\text{Ph}}[\text{P}_2\text{N}_2]\text{NbMe}$ above using 500 mg (0.744 mmol) of $^{\text{Cy}}[\text{P}_2\text{N}_2]\text{NbCl}$ and 0.25 ml of MeMgCl . Yield 412 mg (85%). *Anal.* Calc. for $\text{C}_{25}\text{H}_{57}\text{N}_2\text{NbP}_2\text{Si}_4$: C, 45.99; H, 8.80; N, 4.29. Found: C, 45.69; H, 8.67; N, 4.69%. MS (EI) m/z (%) 652, (80) $[M]^+$. μ_{eff} (Evans method) = $2.5\ \mu_{\text{B}}$.

2.2.3. $^{\text{R}}[\text{P}_2\text{N}_2]\text{NbMe}(\text{py})$ ($\text{R} = \text{Ph}$ (3) or Cy (4))

$^{\text{R}}[\text{P}_2\text{N}_2]\text{NbMe}$ (200 mg) was dissolved in pyridine (5 ml) to give deep indigo and dark purple solutions for **3** and **4**, respectively. Removal of excess pyridine under vacuum allowed quantitative isolation of $^{\text{R}}[\text{P}_2\text{N}_2]\text{NbMe}(\text{py})$ as paramagnetic solids. For $\text{R} = \text{Ph}$, **3**: *Anal.* Calc. for $\text{C}_{30}\text{H}_{50}\text{N}_3\text{NbP}_2\text{Si}_4$: C, 50.05; H, 7.00; N, 5.84. Found: C, 50.09; H, 6.67; N, 5.69%. MS (EI) m/z (%) 719, (10) $[M]^+$. μ_{eff} (Evans method) = $2.5\ \mu_{\text{B}}$. For $\text{R} = \text{Cy}$, **4**: *Anal.* Calc. for $\text{C}_{30}\text{H}_{62}\text{N}_3\text{NbP}_2\text{Si}_4$: C, 49.22; H, 8.54; N, 5.74. Found: C, 49.39; H, 8.64; N, 5.89%. MS (EI) m/z (%) 731, (10) $[M]^+$. μ_{eff} (Evans method) = $2.6\ \mu_{\text{B}}$.

2.2.4. $(^{\text{Ph}}[\text{P}_2\text{N}_2]\text{NbMe})_2(\mu\text{-N}_2)$ (5)

MeMgCl (0.25 ml, 0.76 mmol) was slowly added to a stirred solution of $^{\text{Ph}}[\text{P}_2\text{N}_2]\text{NbCl}$ (500 mg, 0.76 mmol) in toluene (25 ml) under nitrogen to produce an immediate colour change from green to dark purple. Within several minutes the solution turned dark brown. Alternatively, a toluene solution of **1** was exposed to an atmosphere of N_2 causing a colour change from purple to brown. After stirring for a further 6 h, solvents were removed in vacuo to produce a brown residue. Extraction with toluene, filtration through Celite and removal of solvent afforded a diamagnetic brown solid that was washed with hexanes to give an analytically pure product. Crystals suitable for X-ray diffraction were obtained by cooling a saturated 50:50 toluene/hexanes solution to $-40\text{ }^{\circ}\text{C}$. Yield 420 mg (85%). ^1H NMR (C_6D_6 , 500.13 MHz, 300 K): δ 0.12 (s, 12H, SiCH_3CH_3), 0.18 (s, 12H, SiCH_3CH_3), 0.35 (s, 12H, SiCH_3CH_3), 0.40 (s, 12H, SiCH_3CH_3), 1.25 (m, 4H, PCHH), 1.28 (m, 8H, PCHH), 1.37 (m, 4H, PCHH), 1.78 (t, $^3J_{\text{HP}} = 3.27\ \text{Hz}$, 3H, NbCH_3), 7.05 (m, 12H, *meta*, *para*-Ph), 7.76 (m, 8H, *ortho*-Ph). $^{13}\text{C}\{^1\text{H}\}$ NMR (C_6D_6 , 125.76 MHz, 300 K) δ 5.91 (s, 4C, SiCH_3), 6.62 (s, 4C, SiCH_3), 6.67 (s, 4C, SiCH_3), 6.99 (s, 4C, SiCH_3), 20.88 (s, 4C, PCH₂), 21.51 (s, 4C, PCH₂), 88.02 (t, $^2J_{\text{PC}} = 16.2\ \text{Hz}$, 2C, NbCH_3), 128.69 (d, $^3J_{\text{PC}} = 4.7\ \text{Hz}$, 8C, *meta*-Ph), 129.84 (s, 4C, *para*-Ph), 132.59 (d, $^2J_{\text{PC}} = 6.65\ \text{Hz}$, 8C, *ortho*-Ph), 139.23 (d, $^1J_{\text{PC}} = 13.3\ \text{Hz}$, 4C, *ipso*-Ph). $^{31}\text{P}\{^1\text{H}\}$ NMR (C_6D_6 , 202.49 MHz, 300 K) δ 13.11 (s). *Anal.* Calc. for $\text{C}_{50}\text{H}_{90}\text{N}_6\text{Nb}_2\text{P}_4\text{Si}_8$: C, 45.85; H, 6.93; N, 6.42. Found: C, 46.25; H, 7.06; N, 6.40%. MS (EI) m/z (%) 1308, (10) $[M]^+$; 1293, (10) $([M]^+ - \text{Me})$; 1278, (100) $([M]^+ - 2 \times \text{Me})$.

2.2.5. (^{Cy}[P₂N₂]NbMe)₂(μ-N₂) (**6**)

(^{Cy}[P₂N₂]NbMe)₂(μ-N₂) was synthesized according to the procedure used for (^{Ph}[P₂N₂]NbMe)₂(μ-N₂) above using 500 mg of ^{Cy}[P₂N₂]NbCl and 0.25 ml of MeMgCl. Alternatively, a toluene solution of **2** was exposed to an atmosphere of N₂ causing a colour change from purple to brown. Crystals suitable for X-ray diffraction were obtained by cooling a saturated 50:50 toluene/hexanes solution to -40 °C. Yield 400 mg (80%). ¹H NMR (C₆D₆, 500.13 MHz, 300 K): δ 0.36 (s, 12H, SiCH₃CH₃), 0.47 (s, 12H, SiCH₃CH₃), 0.49 (s, 12H, SiCH₃CH₃), 0.56 (s, 12H, SiCH₃CH₃), 0.97, 1.19, 1.42 (m, 44H, PC₆H₁₁), 1.75 (m, 8H, PCHH), 1.94 (m, 4H, PCHH), 3.78 (t, ³J_{HP} = 3.20 Hz, 3H, NbCH₃). ¹³C{¹H} NMR (C₆D₆, 125.76 MHz, 300 K) δ 6.58 (s, 4C, SiCH₃), 6.60 (s, 4C, SiCH₃), 6.80 (s, 4C, SiCH₃), 6.82 (s, 4C, SiCH₃), 13.27 (s, 4C, PCH₂), 13.39 (s, 4C, PCH₂), 25.16 (s, 4C, *para*-Cy), 26.80 (d, ²J_{PC} = 9.56 Hz, 8C, *ortho*-Cy), 27.74 (d, ¹J_{PC} = 10.56 Hz, 4C, *ipso*-Cy), 28.89 (d, ³J_{PC} = 4.78 Hz, 8C, *meta*-Ph), 86.77 (d, ²J_{PC} = 14.8 Hz, 2C, NbCH₃). ³¹P{¹H} NMR (C₆D₆, 202.49 MHz, 300 K): δ 12.1 (s, w_{1/2} = 503 Hz) 21.7 (s w_{1/2} = 534 Hz). *Anal.* Calc. for C₅₀H₁₁₄N₆Nb₂P₄Si₈: C, 45.02; H, 8.61; N, 6.30. Found: C, 45.32; H, 8.63; N, 5.98%. MS (EI) *m/z* (%) 1332, (30) [*M*]⁺; 1302, (2) ([*M*]⁺ - 2 × Me).

2.2.6. (^{Ph}[P₂N₂]Nb)₂(μ-COMe)₂ (**7**)

(^{Ph}[P₂N₂]NbMe)₂(μ-N₂) (300 mg, 0.229 mmol) was dissolved in toluene (20 ml) and degassed by three freeze-pump-thaw cycles. The thawed solution was then placed under 1 atm of CO and stirred for 12 h. All volatiles were removed under vacuum leaving a dark brown paramagnetic residue. Slow evaporation of a hexanes solution yielded dark brown crystals. Yield 260 mg (85%). *Anal.* Calc. for C₅₂H₉₀N₄Nb₂O₂P₄Si₈: C, 46.69; H, 6.78; N, 4.19. Found: C, 43.85; H, 6.86; N, 4.22%. MS (EI) *m/z* (%) 668, (95) ([*M*]⁺ - ^{Ph}[P₂N₂]NbCOMe).

2.2.7. (^{Cy}[P₂N₂]Nb)₂(μ-COMe)₂ (**8**)

(^{Cy}[P₂N₂]Nb)₂(μ-COMe)₂ was synthesized according to the procedure used for (^{Ph}[P₂N₂]Nb)₂(μ-COMe)₂ above using 300 mg (0.230 mmol) of (^{Cy}[P₂N₂]NbMe)₂(μ-N₂). Yield 250 mg (80%). *Anal.* Calc. for C₅₂H₁₁₄N₄Nb₂O₂P₄Si₈: C, 49.55; H, 8.46; N, 3.98. Found C, 49.66; H, 8.59; N, 3.90%. MS (EI) *m/z* (%) 680, (95) ([*M*]⁺ - ^{Cy}[P₂N₂]NbCOMe).

2.2.8. Reaction of (^R[P₂N₂]NbMe)₂(μ-N₂) with H₂

(^R[P₂N₂]NbMe)₂(μ-N₂) (0.229 mmol) was dissolved in toluene (20 ml) and degassed by three freeze-pump-thaw cycles. The thawed solution was then placed under 1 atm of H₂ and stirred for 12 h. All volatiles were removed under vacuum leaving a dark brown paramagnetic residue. Slow evaporation of a toluene solu-

tion yielded dark brown crystals that analyzed for (^R[P₂N₂]Nb)₂(μ-N₂). For R = Ph: Yield 234 mg (80%) *Anal.* Calc. for C₄₈H₈₄N₆Nb₂P₄Si₈: C, 45.05; H, 6.62; N, 6.57. Found C, 44.86; H, 6.47; N, 4.13%. MS (EI) *m/z* (%) 1278, (95) [*M*]⁺. For R = Cy: Yield 245 mg (82%) *Anal.* Calc. for C₄₈H₁₀₈N₆Nb₂P₄Si₈: C, 44.22; H, 8.35; N, 6.45. Found: C, 44.46; H, 8.47; N, 4.43%. MS (EI) *m/z* (%) 1302, (95) [*M*]⁺.

2.2.9. N₂ exchange with (^R[P₂N₂]NbMe)₂(μ-N₂)

(^R[P₂N₂]NbMe)₂(μ-N₂) (0.075 mmol) was dissolved in toluene (10 ml) and degassed by three freeze-pump-thaw cycles. The thawed solution was then placed under 1 atm of ¹⁵N₂ and stirred for 48 h. All volatiles were removed under vacuum. MS (EI) *m/z* (%) For **5**-¹⁵N₂: 1310, (10) [*M*]⁺. For **6**-¹⁵N₂: 1334, (10) [*M*]⁺.

2.2.10. (^{Ph}[P₂N₂]NbMe)₂(μ-N₂) and (^{Cy}[P₂N₂]NbMe)₂(μ-N₂) crossover experiment

(^{Ph}[P₂N₂]NbMe)₂(μ-N₂) (0.075 mmol) and (^{Cy}[P₂N₂]NbMe)₂(μ-N₂) (0.075 mmol) were dissolved in toluene (25 ml) and stirred for 48 h. Removal of solvent allowed isolation of a brown residue. ¹H NMR spectroscopy shows complicated resonances arising from a mixture of **5**, **6**, and (^{Ph}[P₂N₂]NbMe)(μ-N₂)(^{Cy}[P₂N₂]NbMe). In addition to resonances arising from **5** and **6**, the ³¹P{¹H} NMR spectrum shows two peaks resulting from (^{Ph}[P₂N₂]NbMe)(μ-N₂)(^{Cy}[P₂N₂]NbMe). Alternatively, the same product mixture can be obtained by addition of MeMgCl (0.1 ml, 0.33 mmol) to an equimolar mixture of ^{Ph}[P₂N₂]NbCl (0.15 mmol) and ^{Cy}[P₂N₂]NbCl (0.15 mmol) in toluene (20 ml) under N₂. ³¹P{¹H} NMR (C₆D₆, 161.98 MHz, 300 K): δ 12.9 (s), 16.5 (s). MS (EI) *m/z* (%) For (^{Ph}[P₂N₂]NbMe)(μ-N₂)(^{Cy}[P₂N₂]NbMe): 1320, (10) [*M*]⁺.

2.3. X-ray crystallographic analyses of **5** and **6**

Suitable crystals were selected and mounted on a glass fibre using Paratone-N oil and freezing to -100 °C. Measurements were made on a Rigaku/ADSC CCD area detector with graphite monochromated Mo Kα radiation. Crystallographic data appear in Table 1. The data were processed [8] and corrected for Lorentz and polarization effects and absorption. Neutral atom scattering factors for all non-hydrogen atoms were taken from the International Tables for X-ray Crystallography [9,10]. Structures were solved by direct methods [11] and expanded using Fourier techniques [12]. Compound **6** crystallizes with one molecule of hexane included in the asymmetric unit. This, as well as one disordered phenyl ring was refined isotropically. All other non-hydrogen atoms were refined anisotropically. Hydrogen atoms were included but not refined and were fixed in calculated positions with C-H = 0.98 Å.

Table 1
 Crystallographic data^a

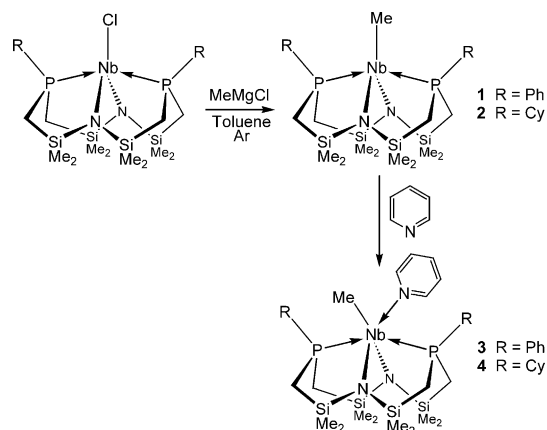
	5	6
Empirical formula	C ₅₀ H ₉₀ N ₆ P ₄ Si ₈ Nb ₂ ·C ₆ H ₁₄	C ₅₀ H ₁₁₄ N ₆ P ₄ Si ₈ Nb ₂
Formula weight	1395.87	1333.88
Colour, habit	brown, block	brown, platelet
Crystal size (mm)	0.30 × 0.30 × 0.20	0.35 × 0.15 × 0.07
Crystal system	monoclinic	monoclinic
Space group	<i>P</i> 2 ₁ / <i>c</i> (#14)	<i>P</i> 2 ₁ / <i>c</i> (#14)
<i>a</i> (Å)	16.033(1)	12.1090(3)
<i>b</i> (Å)	26.351(2)	23.6327(5)
<i>c</i> (Å)	18.940(1)	24.8984(7)
α (°)	90	90
β (°)	113.352(2)	97.468(2)
γ (°)	90	90
<i>V</i> (Å ³)	7346.1(7)	7064.7(3)
<i>Z</i>	4	4
<i>T</i> (°C)	−100 ± 1	−100 ± 1
ρ_{calc} (g cm ^{−3})	1.262	1.254
<i>F</i> (000)	2944.00	2840.00
μ (Mo K α) (cm ^{−1})	5.66	5.86
Transmission factors	0.4065–1.0000	0.7815–1.0000
$2\theta_{\text{max}}$ (°)	50.2	57.4
Total number of reflections	43 746	51 422
Number of unique reflections	12 909	16 109
<i>R</i> _{merge}	0.130	0.054
Number reflections with <i>I</i> ≥ <i>n</i> σ (<i>I</i>)	7450, <i>n</i> = 2	10645, <i>n</i> = 3
Number of variables	643	631
<i>R</i> (<i>F</i> ² , all data)	0.112	0.057
<i>R</i> _w (<i>F</i> ² , all data)	0.183	0.088
<i>R</i> (<i>F</i> , <i>I</i> > 3 σ (<i>I</i>))	0.065	0.030
<i>R</i> _w (<i>F</i> , <i>I</i> > 3 σ (<i>I</i>))	0.162	0.038
Goodness-of-fit	0.85	0.99

^a Rigaku/ADSC CCD diffractometer, $R = \Sigma||F_o^2| - |F_c^2||/\Sigma|F_o^2|$; $R_w = (\Sigma w(|F_o^2| - |F_c^2|)^2/\Sigma w|F_o^2|)^{1/2}$.

3. Results and discussion

3.1. Synthesis of niobium(III) methyl derivatives

The niobium(III) chloride precursors ^R[P₂N₂]NbCl (R = Ph, Cy) react with MeMgCl in toluene to generate the purple niobium methyl complexes ^R[P₂N₂]NbMe (R = Ph, **1**; R = Cy, **2**) (Scheme 1). The choice of alkylating agent appears significant as the use of MeLi produces only intractable products [13]. Methyl complexes **1** and **2** are paramagnetic and solution magnetic susceptibility measurements by the Evans method [14,15] indicate a magnetic moment of 2.5 μ_B for each complex consistent with high spin d² niobium centres. This value is slightly lowered from the predicted spin-only magnetic moment of 2.83 μ_B due to the large spin-orbit coupling effects inherent in niobium systems [16,17]. Unlike the previously reported bulkier monomeric niobium alkyls of [P₂N₂] [6], which are highly



Scheme 1.

soluble in even the most non-polar solvents, the methyl complexes **1** and **2** are insoluble in hexanes. Also, toluene solutions of **1** and **2** show slow decomposition of the methyl complexes. Decomposition of these products can be prevented by the addition of a donor solvent such as pyridine. Thus, the addition of excess pyridine to solutions of **1** and **2** generates ^R[P₂N₂]NbMe(py) (R = Ph, **3**; R = Cy, **4**), which are considerably more stable than the methyl complexes alone. Removal of excess pyridine under vacuum allows the isolation of adducts **3** and **4** as paramagnetic indigo and dark purple solids, respectively. Magnetic moment measurements of **3** and **4** in solution give values of 2.5 and 2.6 μ_B , respectively, again indicating high spin d² metal centres.

Exposure of toluene solutions of **1** and **2** to 1 atm of N₂ causes a rapid colour change from purple to brown. Removal of solvent under vacuum yields the brown diamagnetic dinitrogen complexes (^R[P₂N₂]NbMe)₂(μ -N₂) (R = Ph, **5**; R = Cy, **6**) (Eq. (1)). Toluene solutions of the pyridine adducts **3** and **4** indicate displacement of pyridine under N₂ atmosphere to also form the dinitrogen complexes **5** and **6**, respectively, albeit at much slower rates. The dinitrogen ligand in these derivatives is thermally labile. Heating toluene solutions of these complexes under partially evacuated conditions regenerates purple solutions of the paramagnetic ^R[P₂N₂]NbMe complexes.

Crystals of **5** and **6** suitable for X-ray diffraction were obtained by cooling saturated 50:50 toluene/hexanes solutions to −40 °C. The structures of the dinitrogen complexes were determined unequivocally by single crystal X-ray structural analysis. The structure of complex **5** is shown in Fig. 1; crystallographic data are given in Table 1 and selected bond lengths, angles and torsion angles in Table 2. The phenyl ring attached to P(2) is disordered and was refined isotropically. The niobium bound methyl group, C(50), appears to have a steric interaction with this phenyl group and is itself affected by this disorder as shown by the large thermal

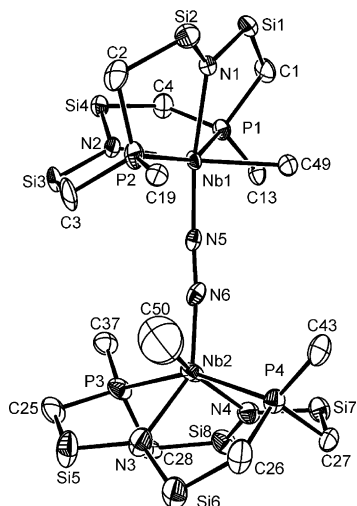
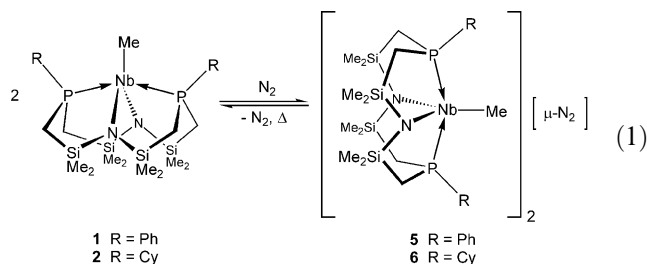


Fig. 1. Molecular structure (ORTEP) of $(^{\text{Ph}}[\text{P}_2\text{N}_2]\text{NbMe})_2(\mu\text{-N}_2)$ (**5**). Silyl methyl groups are omitted for clarity and only *ipso* carbons of phenyl rings are shown.

ellipsoid; a close contact of 0.975 Å is observed between H atoms on the phenyl and methyl groups. The molecular structure clearly indicates the presence of an end-on bridging N_2 unit. The geometries surrounding each niobium centre are different. Nb(1) occupies a distorted octahedral geometry with the $[\text{P}_2\text{N}_2]$ phosphine donors, P(1) and P(2), residing *trans* to each other while the amide donors, N(1) and N(2), lie in *cis* orientation. The methyl, C(49), and dinitrogen, N(5), ligands complete the coordination sphere and lie *cis* to one another. The coordination environment of Nb(2) is much more distorted and is better described as a capped trigonal bipyramid. P(3) and P(4) of the $[\text{P}_2\text{N}_2]$ macrocycle occupy axial positions. As is observed in other early transition metal complexes of $[\text{P}_2\text{N}_2]$, the P–Nb–P angles of the phosphine donors are slightly pinched back

from the ideal 180° angle. The two amide donors, N(3) and N(4), and the dinitrogen ligand, N(6), reside in equatorial positions. The sum of the N(3)–Nb(2)–N(4), N(4)–Nb(2)–N(6), and N(3)–Nb(2)–N(6) bond angles is 359.65° and indicates an ideal trigonal planar arrangement. The remaining methyl ligand, C(50), caps the face defined by N(3), P(4), and N(6) and causes inequivalent phosphorus environments for P(3) and P(4). The two Nb–C bond lengths are different; Nb(1)–C(49) is 2.209(6) Å while Nb(2)–C(50) is 2.338(13) Å.



The structure of complex **6** is shown in Fig. 2; crystallographic data are given in Table 1 and selected bond lengths, angles and torsion angles in Table 3. The crystal structure of **6** is more symmetrical than that of **5**, that is, both niobium centres occupy distorted octahedral geometries. The macrocycle forces the methyl and dinitrogen ligands into *cis* orientation as observed in the coordination environment of Nb(1) in complex **5**. The $[\text{P}_2\text{N}_2]$ ligands on each niobium lie skewed from one another along the Nb– N_2 –Nb axis. The niobium–methyl groups, therefore, are rotated approximately 125° from one another. The binding of the end-on bridging dinitrogen moiety is slightly bent in both compounds with Nb(1)–N(5)–N(6) and Nb(2)–N(6)–N(5) angles of $174.5(4)$ and $172.6(5)^\circ$, respectively, in **5** and $175.4(2)^\circ$ and $173.7(2)^\circ$, respectively, in **6**. The Nb–

Table 2
Selected bond lengths (Å) and angles ($^\circ$) in $(^{\text{Ph}}[\text{P}_2\text{N}_2]\text{NbMe})_2(\mu\text{-N}_2)$ (**5**)

Bond lengths			
Nb(1)–N(1)	2.263(5)	Nb(1)–N(2)	2.153(5)
Nb(1)–P(1)	2.5807(17)	Nb(1)–P(2)	2.6110(17)
Nb(1)–N(5)	1.869(5)	Nb(1)–C(49)	2.209(6)
N(5)–N(6)	1.280(7)	Nb(2)–N(3)	2.177(6)
Nb(2)–N(4)	2.166(6)	Nb(2)–N(6)	1.840(6)
Nb(2)–P(3)	2.5879(18)	Nb(2)–P(4)	2.5881(17)
Nb(2)–C(50)	2.338(13)		
Bond angles			
N(1)–Nb(1)–N(2)	93.82(19)	P(1)–Nb(1)–P(2)	155.85(2)
N(3)–Nb(2)–N(4)	105.2(2)	P(3)–Nb(2)–P(4)	156.01(6)
Nb(1)–N(5)–N(6)	174.5(4)	Nb(2)–N(6)–N(5)	172.6(5)
N(5)–Nb(1)–C(49)	87.2(2)	N(6)–Nb(2)–C(50)	75.0(4)
N(1)–Nb(1)–N(5)	166.8(2)	N(2)–Nb(1)–N(5)	97.8(2)
N(3)–Nb(2)–N(6)	141.1(2)	N(4)–Nb(2)–N(6)	113.4(2)
Nb(1)–N(5)–N(6)–Nb(2)	90(5)	C(49)–Nb(1)–N(5)–N(6)	54(4)
C(50)–Nb(2)–N(6)–N(5)	–35(4)		

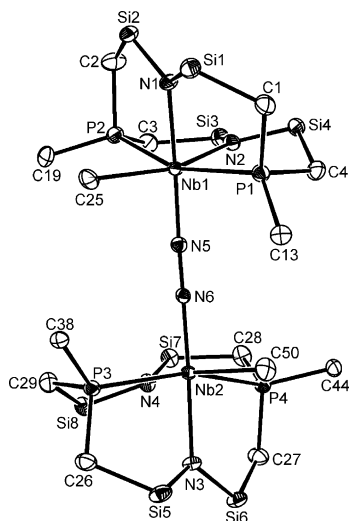


Fig. 2. Molecular structure (ORTEP) of $(^{\text{Cy}}[\text{P}_2\text{N}_2]\text{NbMe})_2(\mu\text{-N}_2)$ (**6**). Silyl methyl groups are omitted for clarity and only phosphorus bound carbons of cyclohexyl rings are shown.

C bond lengths in **6** are experimentally identical; Nb(1)–C(25) possesses a bond distance of 2.206(3) Å while Nb(2)–C(50) is 2.200(3) Å. These distances are equivalent to the Nb(1)–C(49) bond length in **5**. The dinitrogen ligands themselves display N–N bond lengths of 1.280(7) Å in **5** and 1.250(3) Å in **6**.

Assignment of formal oxidation states to the bridging dinitrogen unit and the niobium centres is challenging. The diamagnetic nature of these species can be most easily reconciled by describing each niobium centre as formally Nb(V) (d^0) whereby the dinitrogen moiety has undergone a four-electron reduction to form a hydrazido (N_2) $^{4-}$ unit. Other niobium dinitrogen complexes have been reported where N–N bond lengths of this magnitude have been described as formally single bond in nature [5,18–21]. However, as indicated above, the

N–N bond lengths lie in the 1.25–1.28 Å range and are more typical of N=N double bonds (compared to PhN=NPh for which the N–N distance is 1.255 Å) [22–25]. This suggests a two-electron reduction of N_2 resulting in a formally diazenido (N_2) $^{2-}$ fragment bridging two Nb(IV) (d^1) centres [26]. This description would implicate strong anti-ferromagnetic coupling between the two d^1 metal centres in order to achieve the observed diamagnetic nature of the complexes [5]. Alternatively, these complexes may be assigned low spin Nb(III) (d^2) oxidation states with the N_2 moiety acting as a neutral, strong field ligand. The N–N bond length of the ligand is considerably elongated from that of free N_2 (where a N–N bond length of ca. 1.1 Å is observed), however, the labile nature of the N_2 fragment under elevated temperature is characteristic of such weakly activated dinitrogen complexes [1–3]. The degree of N_2 reduction in end-on bonded dinitrogen complexes is not easily deduced from N–N bond length alone [27].

3.2. Variable-temperature NMR spectroscopy of $(^{\text{R}}[\text{P}_2\text{N}_2]\text{NbMe})_2(\mu\text{-N}_2)$ ($\text{R} = \text{Ph}, \text{Cy}$)

The relatively simple room temperature ^1H and $^{31}\text{P}\{^1\text{H}\}$ NMR spectra of **5** suggest a molecule of higher symmetry than observed in the solid-state structure. The ^1H NMR spectrum of **5** at room temperature displays four silyl methyl resonances and four sets of methylene proton resonances. The niobium methyl proton resonance appears as a triplet at 1.78 ppm due to coupling to two equivalent ^{31}P nuclei. This was confirmed by the $^1\text{H}\{^{31}\text{P}\}$ spectrum where a singlet is observed for the methyl resonance. The $^{13}\text{C}\{^1\text{H}\}$ chemical shift of the methyl group is observed as a triplet at 88.02 ppm, again indicating coupling to two equivalent ^{31}P nuclei with $^2J_{\text{PC}} = 16.2$ Hz. The $^{31}\text{P}\{^1\text{H}\}$ spectrum displays a single

Table 3
Selected bond lengths (Å) and angles (°) in $(^{\text{Cy}}[\text{P}_2\text{N}_2]\text{NbMe})_2(\mu\text{-N}_2)$ (**6**)

Bond lengths			
Nb(1)–N(1)	2.234(2)	Nb(1)–N(2)	2.184(2)
Nb(1)–P(1)	2.6571(7)	Nb(1)–P(2)	2.5800(7)
Nb(1)–N(5)	1.868(2)	Nb(1)–C(25)	2.206(3)
N(5)–N(6)	1.250(3)	Nb(2)–N(3)	2.214(2)
Nb(2)–N(4)	2.189(2)	Nb(2)–N(6)	1.875(2)
Nb(2)–P(3)	2.6391(7)	Nb(2)–P(4)	2.5853(7)
Nb(2)–C(50)	2.200(3)		
Bond angles			
N(1)–Nb(1)–N(2)	94.65(8)	P(1)–Nb(1)–P(2)	160.69(2)
N(3)–Nb(2)–N(4)	93.59(6)	P(3)–Nb(2)–P(4)	159.26(2)
Nb(1)–N(5)–N(6)	175.4(2)	Nb(2)–N(6)–N(5)	173.7(2)
N(5)–Nb(1)–C(25)	89.5(1)	N(6)–Nb(2)–C(50)	88.7(1)
N(1)–Nb(1)–N(5)	164.26(8)	N(2)–Nb(1)–N(5)	98.05(8)
N(3)–Nb(2)–N(6)	164.42(8)	N(4)–Nb(2)–N(6)	99.07(8)
Nb(1)–N(5)–N(6)–Nb(2)	27(4)	N(6)–N(5)–Nb(1)–C(25)	–91(2)
N(5)–N(6)–Nb(2)–C(50)	–62(2)		

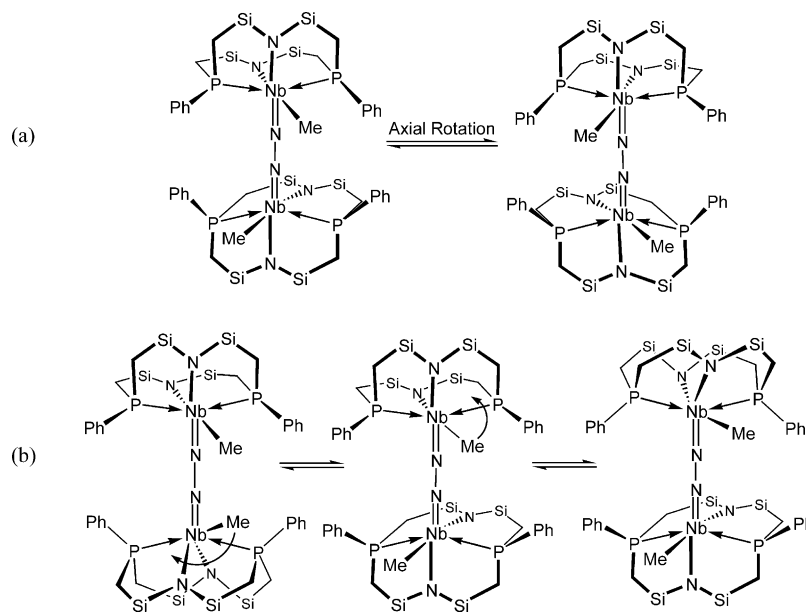


Fig. 3. (a) Racemization via axial rotation about the Nb–N₂–Nb axis assuming two octahedral Nb centres in solution. (b) Isomerization via methyl group migration between capped trigonal bipyramidal and octahedral geometries in (^{Ph}[P₂N₂]NbMe)₂(μ-N₂) (**5**). Methyl groups on silicon are omitted for clarity.

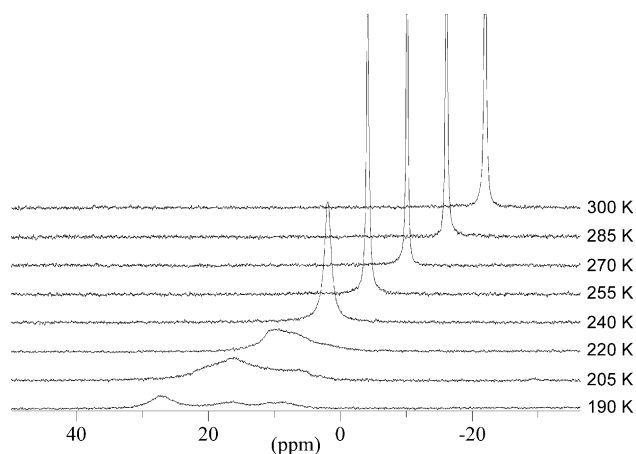


Fig. 4. Variable-temperature ³¹P{¹H} NMR spectra of (^{Ph}[P₂N₂]NbMe)₂(μ-N₂) (**5**).

resonance at 13.1 ppm indicating four equivalent phosphorus centres. This last result contrasts the solid state structure shown in Fig. 1 wherein all four phosphorus donors reside in chemically inequivalent environments. It is evident, therefore, that in solution some fluxional process is operative. The following are two possible rationalizations of the different solution and solid state structures. First, the different geometries at each niobium centre seen in the molecular structure of **5** may be a solid state effect, which, in solution converts into two staggered octahedral geometries as observed in the solid state molecular structure for **6**. The resulting phosphorus environments become equivalent if one assumes an unhindered rotation about the Nb–N₂–Nb

axis (Fig. 3(a)). The other possibility is that in solution the mixed geometries of the niobium centres are identical to that observed in the solid-state structure, but a more complicated process ensues. Exchange of the phosphorus environments occurs by a process where the methyl group shifts from one face to another, likely via an octahedral intermediate as shown in Fig. 3(b). In this case, once both centres are octahedral, rotation about the Nb–N₂–Nb axis can occur followed by methyl migration on the opposite niobium centre. Variable temperature NMR studies were performed on a degassed sample that was sealed under vacuum. As the temperature is lowered, the ³¹P{¹H} NMR signal broadens and then decoalesces at 220 K. The low-temperature spectrum at 190 K consists of three broad resonances at 30.14, 19.60 and 12.61 ppm. The large quadrupole moment of the ⁹³Nb nucleus is also a likely source of increased line broadening of the resonances at low temperatures. The effect of temperature on the

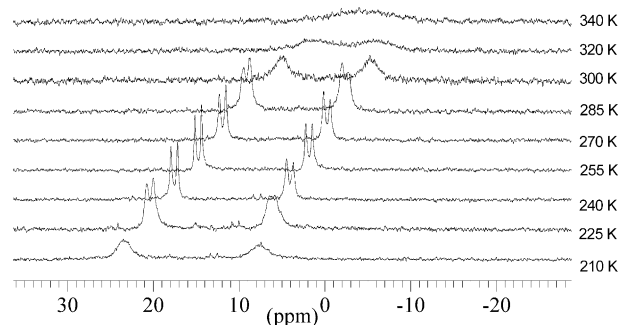


Fig. 5. Variable-temperature ³¹P{¹H} NMR spectra of (^{Cy}[P₂N₂]NbMe)₂(μ-N₂) (**6**).

$^{31}\text{P}\{\text{H}\}$ spectrum of $(^{\text{Ph}}[\text{P}_2\text{N}_2]\text{NbMe})_2(\mu\text{-N}_2)$ is shown in Fig. 4.

A variable temperature ^1H NMR spectroscopy study of **5** was also conducted. As the temperature was lowered to 190 K the resonances, most notably those of the silyl methyl and niobium bound methyl groups, began to broaden. The low symmetry of the solid state molecular structure suggests that each of the silyl methyl groups would effectively be inequivalent giving rise to 16 resonances. However, over the temperature range from 300 to 190 K only four silyl methyl resonances are ever observed and no low-temperature limiting spectrum indicating the lack of symmetry present in the solid state could be obtained.

The room temperature ^1H NMR spectrum of **6** is similar to that of **5**, albeit for the presence of cyclohexyl rather than phenyl resonances. As in complex **5**, four sets of silyl methyl groups are detected. However, the niobium methyl resonance occurs at 3.78 ppm, slightly further downfield from that observed in **5**. Coupling to two equivalent ^{31}P nuclei is also observed giving rise to a triplet. The $^{13}\text{C}\{\text{H}\}$ chemical shift of the methyl group is observed as a triplet at 86.77 ppm coupled to two equivalent ^{31}P nuclei with $^2J_{\text{PC}} = 14.8$ Hz.

The room temperature $^{31}\text{P}\{\text{H}\}$ spectrum of **6** differs from that of **5**. Rather than a single peak, two broad resonances are observed at 12.1 and 21.7 ppm, consistent with inequivalent environments. As the temperature is lowered to 255 K, these resonances sharpen and resolve into a pair of doublets at 12.1 and 21.7 ppm, with $^2J_{\text{PP}} = 155.9$ Hz, which is consistent with two transdisposed phosphorus environments on the same metal centre. Lowering the temperature further causes loss of coupling resolution. As the temperature is raised to 360 K, the two broad signals appear to coalesce into a single broad resonance then disappear. This line broadening likely arises from the fast N_2 dissociation and reassociation and from the presence of the resulting paramagnetic niobium(III) methyl species. The effect of temperature on the $^{31}\text{P}\{\text{H}\}$ spectrum of **6** is shown in Fig. 5.

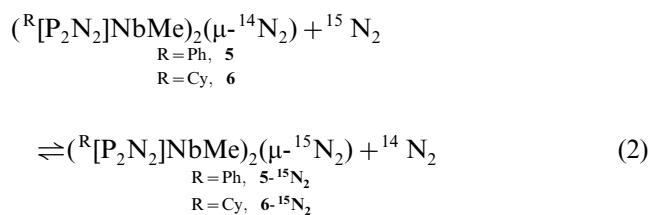
Above 340 K both **5** and **6** show N_2 dissociation and association (where very broad peaks are observed in the $^{31}\text{P}\{\text{H}\}$ spectra). Raising the temperature further causes total absence of resonances in the $^{31}\text{P}\{\text{H}\}$ NMR spectra indicating dissociation of the N_2 to generate the paramagnetic $^{\text{R}}[\text{P}_2\text{N}_2]\text{NbMe}$ species (see below). The presence of inequivalent phosphorus environments in **6** arises from a less energetically accessible rotation about the Nb– N_2 –Nb axis due to the increased bulk of the cyclohexyl moieties, which locks **6** into one of two enantiomers (Fig. 3a). It is possible that the phenyl groups may be capable of rotating past each other because of the favourability of π – π stacking which is not possible for the cyclohexyl substituents. Racemization by the mechanisms proposed for

$(^{\text{Ph}}[\text{P}_2\text{N}_2]\text{NbMe})_2(\mu\text{-N}_2)$ (**5**) is not observed in **6**. The low-temperature $^{31}\text{P}\{\text{H}\}$ NMR data suggest that rotation around the Nb– N_2 –Nb axis is hindered giving rise to two inequivalent phosphorus centres; one phosphorus environment is eclipsed by the Nb–Me group while the other is eclipsed by an amido nitrogen of the $[\text{P}_2\text{N}_2]$ ligand. If free rotation about the Nb– N_2 –Nb axis was occurring, the phosphorus environments would remain identical and a single resonance would be observed as for **5**. Again, quadrupolar effects of the ^{93}Nb nucleus may also contribute to line broadening at lower temperatures.

3.3. Dinitrogen exchange and crossover in **5** and **6**

While the paramagnetic methyl complexes **1** and **2** readily react with N_2 at ambient temperature to form diamagnetic dinitrogen complexes, heating toluene solutions of **5** and **6** above 360 K under partial vacuum shows loss of signal in their respective $^{31}\text{P}\{\text{H}\}$ NMR spectra. The ^1H NMR spectra also show broadened and shifted resonances indicative of the presence of paramagnetic species. The samples are also observed to revert to the purple colour characteristic of the paramagnetic methyl complexes, **1** and **2**. These observations indicate that dissociation of the dinitrogen ligand can be induced thermally (Eq. (1)). Cooling the samples to 300 K causes reappearance of brown solutions characteristic of the dinitrogen complexes and confirmed by their respective ^1H and $^{31}\text{P}\{\text{H}\}$ NMR spectra.

That the dinitrogen ligand in **5** and **6** is labile is supported by exchange experiments utilizing $^{15}\text{N}_2$ (Eq. (2)). A toluene solution of **5** was degassed and then blanketed with one atm of $^{15}\text{N}_2$. The solution was then stirred for 72 h before removal of all volatiles under vacuum. This procedure was repeated for **6**. Characterization by mass spectrometry shows the presence of parent peaks corresponding to $(^{\text{R}}[\text{P}_2\text{N}_2]\text{NbMe})_2(^{15}\text{N}_2)$ (R = Ph, **5**- $^{15}\text{N}_2$ and Cy, **6**- $^{15}\text{N}_2$) in addition to those of the non-labelled species. The intensities of the peaks were identical for both the naturally abundant and isotopically enriched species suggesting a 1:1 mixture. ^{15}N NMR spectra for **5**- $^{15}\text{N}_2$ and **6**- $^{15}\text{N}_2$ were unobservable, likely because of line broadening resulting from the quadrupolar ^{93}Nb nucleus. Also, coupling to ^{15}N could not be determined in the $^{31}\text{P}\{\text{H}\}$ NMR spectrum due to already broad line widths.



species. The pentacoordinate niobium–methyl complexes show a propensity for dinitrogen activation and generate diamagnetic dinuclear organoniobium dinitrogen complexes, which contain end-on bound N₂ fragments as elucidated by X-ray molecular structure determination. Variable-temperature ¹H and ³¹P{¹H} NMR spectroscopies indicate fluxional processes in dinitrogen complex **5**. In the solid state, **5** possesses different coordination geometries at each niobium atom. One niobium occupies an octahedral coordination environment and the second niobium centre occupies a capped trigonal bipyramidal geometry. Exchange in **5** can proceed via rearrangement in solution to generate two octahedral niobium centres with rotation about the Nb–N₂–Nb axis. In the absence of this geometric rearrangement, a methyl group migration followed by axial rotation would result in equivalent phosphorus environments. Complex **6** appears to be locked with respect to axial rotation resulting in inequivalent phosphorus centres that appear as two doublets in its ³¹P{¹H} NMR spectrum. Whereas the planar phenyl substituents are capable of rotating past each other in a “gear-like” fashion, the increased bulk of the cyclohexyl substituents is believed to hinder rotation about the Nb–N₂–Nb axis.

5. Supplementary material

Complete crystallographic data including ORTEP diagrams, bond lengths and angles, final atomic coordinates and equivalent isotropic thermal parameters, anisotropic thermal parameters, intermolecular contacts and least-squares planes for complexes **5** and **6** have been deposited with the Cambridge Crystallographic Data Centre, CCDC Nos. 184666 and 184667. Copies of this information may be obtained free of charge from The Director, CCDC, 12 Union Road, Cambridge CB2 1EZ, UK (fax: +44-1223-336-033; e-mail: deposit@ccdc.cam.ac.uk or www: <http://www.ccdc.cam.ac.uk>).

Acknowledgements

We thank NSERC of Canada for funding.

References

- [1] M.D. Fryzuk, S.A. Johnson, *Coord. Chem. Rev.* 200–202 (2000) 379.

- [2] S. Gambarotta, *J. Organomet. Chem.* 500 (1995) 117.
 [3] M. Hidai, Y. Mizobe, *Chem. Rev.* 95 (1995) 1115.
 [4] M.D. Fryzuk, C.M. Kozak, P. Mehrhodavandi, L. Morello, B.O. Patrick, S.J. Rettig, *J. Am. Chem. Soc.* 124 (2002) 516.
 [5] M.D. Fryzuk, C.M. Kozak, M.R. Bowdridge, B.O. Patrick, S.J. Rettig, *J. Am. Chem. Soc.* 124 (2002) 8389.
 [6] M.D. Fryzuk, C.M. Kozak, M.R. Bowdridge, W. Jin, D. Tung, B.O. Patrick, S.J. Rettig, *Organometallics* 20 (2001) 3752.
 [7] A.B. Pangborn, M.A. Giardello, R.H. Grubbs, R.K. Rosen, F.J. Timmers, *Organometallics* 15 (1996) 1518.
 [8] teXsan Crystal Structure Analysis Package, Molecular Structure Corp., The Woodlands, TX, 1995.
 [9] *International Tables for X-ray Crystallography*, vol. C, Kluwer Academic, Boston, MA, 1992, pp. 200–206.
 [10] *International Tables for X-ray Crystallography*, vol. IV, Kynoch Press, Birmingham, UK (present distributor Kluwer Academic, Boston, MA), 1974, pp. 99–102.
 [11] A. Altomare, M.C. Burla, G. Cammali, M. Cascarano, C. Giacovazzo, A. Guagliardi, A.G.G. Moliterni, G. Polidori, A. Spagna, SIR97: A New Tool for Crystal Structure Determination and Refinement, 1999.
 [12] P.T. Beurskens, G. Admiraal, G. Beurskens, W.P. Bosman, R. de Gelder, R. Israel, J.M.M. Smits, DIRDIF94; The DIRDIF-94 program system, Technical Report of the Crystallography Laboratory, University of Nijmegen, Nijmegen, The Netherlands, 1994.
 [13] M.D. Fryzuk, J.B. Love, S.J. Rettig, *Organometallics* 17 (1998) 846.
 [14] D.F. Evans, *J. Chem. Soc.* (1959) 2003.
 [15] S.K. Sur, *J. Magn. Res.* 82 (1989) 169.
 [16] O. Kahn, *Molecular Magnetism*, VCH, New York, 1993.
 [17] R.L. Carlin, *Magnetochemistry*, Springer-Verlag, Heidelberg, 1986.
 [18] M.D. Fryzuk, S.A. Johnson, B.O. Patrick, A. Albinati, S.A. Mason, T.K. Koetzle, *J. Am. Chem. Soc.* 123 (2001) 3960.
 [19] A. Caselli, E. Solari, R. Scopelliti, C. Floriani, N. Re, C. Rizzoli, A. Chiesi-Villa, *J. Am. Chem. Soc.* 122 (2000) 3652.
 [20] P. Berno, S. Gambarotta, *Organometallics* 14 (1995) 2159.
 [21] J.R. Dilworth, R.A. Henderson, A. Hills, D.L. Hughes, C. MacDonald, A.N. Stephens, D.R.M. Walton, *J. Chem. Soc., Dalton Trans.* (1990) 1077.
 [22] C.J. Brown, *Acta Crystallogr.* 21 (1966) 146.
 [23] J.A. Bouwstra, A. Schouten, J. Kroon, *Acta Crystallogr., C* 39 (1983) 1121.
 [24] L.E. Sutton, *Tables of Interatomic Distances and Configuration in Molecules and Ions*; Chemical Society Special Publication No. 11, Chemical Society, London, 1958.
 [25] A. Mostad, C. Romming, *Acta Chem. Scand.* 25 (1971) 3561.
 [26] For a heterodinuclear niobium/molybdenum dinitrogen complex see: D.J. Mindiola, K. Meyer, J.P.F. Cherry, T.A. Baker, C.C. Cummins, *Organometallics* 19 (2000) 1622.
 [27] G.J. Leigh, *Acc. Chem. Res.* 25 (1992) 177.
 [28] P.J. Chirik, L.M. Henling, J.E. Bercaw, *J. Am. Chem. Soc.* 20 (2001) 534.
 [29] S.K. Hao, P. Berno, R.K. Minhas, S. Gambarotta, *Inorg. Chim. Acta* 244 (1996) 37.
 [30] M.E. Kerr, N. Sarker, A.S. Hneihen, G.K. Schulte, J.W. Bruno, *Organometallics* 19 (2000) 901.